RSC Advances

PAPER

View Article Online
View Journal | View Issue

Cite this: *RSC Adv.*, 2017, **7**, 2773

Synthesis of a Fe_3O_4@P4VP@metal–organic framework core–shell structure and studies of its aerobic oxidation reactivity†

Zongcheng Miao,[a] Xin Shu*[b] and Daniele Ramella[c]

Received 25th October 2016
Accepted 12th December 2016

DOI: 10.1039/c6ra25820d

www.rsc.org/advances

A novel core–shell magnetic Fe_3O_4@P4VP(poly(4-vinylpyridine))@MIL-100(Fe) composite material has been successfully synthesized. The Fe_3O_4@P4VP core was initially prepared *via* polymerization of P4VP on the surface of pre-made Fe_3O_4 microspheres. The MIL-100(Fe) (MIL, Matérial Institut Lavoisier) metal–organic framework shell was then introduced through a layer by layer strategy. The obtained Fe_3O_4@P4VP@MIL-100(Fe) catalyst was applied in the selective oxidation of alcohols using molecular oxygen as the oxidant, and a variety of substrates were tolerated. The initial activity of the Fe_3O_4@P4VP@MIL-100(Fe) core–shell catalyst was maintained after ten reuses.

1. Introduction

Catalytic oxidations, such as conversions of alcohols to their corresponding carbonyl compounds, are of considerable importance in fine and industrial organic chemistry.[1] Recently, aerobic transition metal-promoted selective oxidations have received increasing attention because of the inexpensiveness and environmental friendliness of molecular oxygen.[2] Studies about homogenous catalysts are abundant in the literature.[3] However, homogeneous catalysts are inherently difficult to recover from the reaction mixture, causing industrial wastes and additional costs.[4] For this reason, heterogeneous catalysts are preferable for organic transformations, as they display several advantages during the purification and recovery steps of products and catalysts.[5]

As a result, numerous heterogeneous catalysts, such as molecular sieve,[6] polymer supported[7] and inorganic microspheres supported ones, have been developed in recent years.[8] Among these solid catalysts, core–shell structured ones have been considered the most ideal ones, thanks to their unique physicochemical and multi-functional properties.[9] Core–shell structures bearing magnetic functionality are of particular interest as an effective separation method because of their easy and quick response in an external magnetic field.[10] A variety of magnetic core–shell composites have been developed utilizing different coatings, such as silica, carbon, polymer and porous materials on a Fe_3O_4 core.[11] Several hybrid magnetic core–shell nanocatalysts have been utilized in a variety of catalytic reactions including reductions, oxidations, epoxidations, coupling reactions and photocatalysis.[12] Many studies have reported immobilization of transition metal salts into core–shell structures.[13] On the other hand, significant metal leaching and poor catalyst recyclability have been recurring issues in these metal immobilized systems. It is difficult to address such limitations because of the low molecular interactions present in the coordination bonds between the metal and the core–shell structure (Scheme 1).[14]

Metal–organic frameworks (MOFs)[15] have gained increasing focus in catalysis, as a kind of porous materials with extremely large surface area, a high number of active sites and good stability.[16] Therefore, fabrication of MOFs coated magnetic core–shell catalysts could address the problem of catalyst leaching and the need for recyclability.[17] In this work, we wish to report a core–shell–shell structured Fe_3O_4@P4VP@MIL-100(Fe)

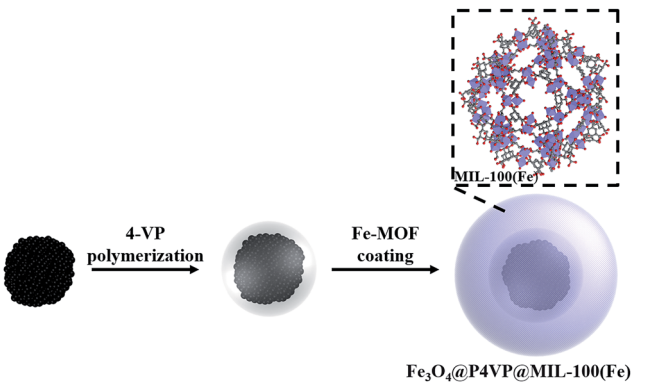

Scheme 1 Schematic illustration of the synthesis of Fe_3O_4@P4VP@MIL-100(Fe).

[a]*Xijing University, Xi'an, Shaanxi Province, 710123, P. R. China*
[b]*College of Science, Beijing University of Chemical Technology, Beijing 100029, P. R. China. E-mail: shuxin@mail.buct.edu.cn*
[c]*Temple University-Beury Hall, 1901, N. 13th Street, Philadelphia, PA 19122, USA*

† Electronic supplementary information (ESI) available. See DOI: 10.1039/c6ra25820d

catalyst, which was assembled by coating MIL-100(Fe) on the surface of Fe_3O_4@P4VP microspheres.[18] The inner shell of the P4VP polymer layer played an important role in the absorption of Fe^{3+} ions for the formation of the MIL-100(Fe) shell, as well as in protecting the magnetic core from destruction and aggregation during the oxidation process. The synthesized Fe_3O_4@P4VP@MIL-100(Fe) was characterized by TEM, field-emission SEM (FESEM), powder X-ray diffraction (PXRD), nitrogen adsorption/desorption analysis, FTIR spectroscopy, thermogravimetric analysis (TGA) and vibrating sample magnetometry (VSM). The aerobic oxidation of alcohols was investigated using our synthesized Fe_3O_4@P4VP@MIL-100(Fe) catalyst and great yields were achieved. A variety of alcohols was compatible with our oxidation system and the core–shell catalyst could be rapidly separated by an externally applied magnetic field.

2. Experimental section

2.1 Materials

Ferric chloride hexahydrate ($FeCl_3 \cdot 6H_2O$), polyvinyl pyrrolidone (PVP; $M_w = 58\,000$), 4-vinyl pyridine (4-VP, 96%), divinylbenzene (DVB, 80%), 1,3,5-benzenetricarboxylic acid (H_3BTC), potassium persulfate (KPS, 99%), 2,2,6,6-tetramethyl-1-piperidinyloxy (TEMPO), trimethylacetaldehyde, benzyl alcohol, substituted benzyl alcohols, 2-pyridinemethanol, cinnamic alcohol, 3-methyl-2-buten-1-ol, 3-methyl-2-buten-1-ol, 1-octyl alcohol, 1-phenylethanol, 2-cyclohexen-1-ol, cyclopentanol, cyclooctene, cyclohexene, cyclododecene, norbornene and α-pinene were purchased from Alfa Aesar. Poly(acrylic acid) (PAA; $M_w = 1800$) was obtained from Sigma-Aldrich. Anhydrous ethanol, ethylene glycol (EG), sodium acetate and potassium nitrite were purchased from Beijing Chemical Reagents Company (China). 4-Vinyl pyridine was purified by distillation under reduced pressure to remove inhibitor hydroquinone before use.

2.2 Synthesis of Fe_3O_4 nanoparticles with PAA

The Fe_3O_4 nanoparticles modified on the surface with poly (acrylic acid) (PAA) were synthesized by solvothermal method according to reported literature. Firstly, $FeCl_3 \cdot 6H_2O$ (1.08 g) and PAA (0.108 g) were dissolved in ethylene glycol (40 mL) under magnetic stirring at 60 °C, followed by adding sodium acetate (9 g) under vigorous stirring to form a uniform solution. Then, the solution was decanted to a stainless-steel autoclave with Teflon-lining (50 mL) and maintained at 200 °C for 12 h. After the autoclave was cooled to room temperature, the black product was collected using a magnet. The Fe_3O_4 nanoparticles modified with PAA were washed with deionized water and ethanol several times, collected and dried under vacuum.

2.3 Preparation of core–shell Fe_3O_4@P4VP microspheres

The core–shell Fe_3O_4@P4VP microspheres were prepared by coating P4VP shell on the surface of Fe_3O_4 nanoparticles through radical initiated polymerization. Fe_3O_4 nanoparticles modified with PAA (0.1 g) were dispersed in 100 mL of a 0.15 wt% PVP aqueous solution under ultrasonication. The uniform solution was mixed with emulsion of 4-VP (0.125 g) and DVB (0.125 g) in aqueous solution (20 mL) that contains PVP (0.05 g). Then it was emulsionized by ultrasonic after placed in a 250 mL four-necked flask. The liquid was mechanical stirred for 4 hours under a flow of nitrogen and then polymerization of 4-VP was initiated by KPS (10 mg); at this point, the solution was heated to 70 °C. Core–shell Fe_3O_4@P4VP microspheres were obtained after 4 h, washed with deionized water and ethanol three times and dried under vacuum.

2.4 Synthesis of core–shell–shell Fe_3O_4@P4VP@MIL-100(Fe) microspheres

The core–shell–shell Fe_3O_4@P4VP@MIL-100(Fe) microspheres were synthesized by a step-by-step strategy. Typically, 0.05 g of Fe_3O_4@P4VP microspheres were dispersed in 10 mL of a 4.0 mM $FeCl_3 \cdot 6H_2O$ ethanol solution for 15 minutes and collected with a magnet. Then the microspheres were dispersed in a H_3BTC ethanol solution (4 mL, 10 mM) and stirred at 70 °C for 30 minutes. The product was washed with ethanol and vacuum dried after twenty cycles.

2.5 Typical catalytic procedure for aerobic oxidation of alcohol

Alcohol (1.0 mmol), Fe_3O_4@P4VP@MIL-100(Fe) catalyst (5 mol%) were mixed in acetonitrile (5 mL); TEMPO (0.5 equiv.) and KNO_2 (0.2 equiv.) were added in a 25 mL flask equipped with a condenser. The catalytic reaction was stirred at 75 °C under 1 atm of O_2. After the reaction, the Fe_3O_4@P4VP@MIL-100(Fe) catalyst was recovered by applying an external magnetic field and the yield of product was determined by GC-MS.

2.6 Leaching test and catalyst recycling

The hot filtration test for the aerobic oxidation of benzyl alcohol was performed on a sample taken from the mixture after letting the reaction run for 4 hours. The catalyst was separated by a magnet and the supernatant solution was transferred into a new flask letting the reaction continue in absence of the catalyst. After certain reaction time, the reaction solution was analyzed by GC-MS. The recyclability of the heterogeneous catalyst was tested for the oxidation of alcohols and epoxidation of olefins. The reaction run with a batch of recycled catalyst was performed under the conditions described above.

3. Results and discussion

The Fe_3O_4 microspheres modified with PAA were synthesized by a solvothermal method reported in literature.[19] These microspheres were composed of tiny Fe_3O_4 nanocrystals within 10 nm (Fig. 1a). The P4VP shell was successfully grafted on Fe_3O_4 to form core–shell composite microspheres held together by hydrogen bonds between carboxyl groups of PAA chains and pyridine. The diameters of the magnetic core and polymer shell were about 200 and 38 nm, respectively (Fig. 1b). Fe_3O_4@P4VP@MIL-100(Fe) core–shell–shell catalysts were prepared by a layer-by-layer method with 5 to 20 assembling cycles (Fig. 1c–f). The Fe^{3+} ions were adsorbed on the surface of P4VP through

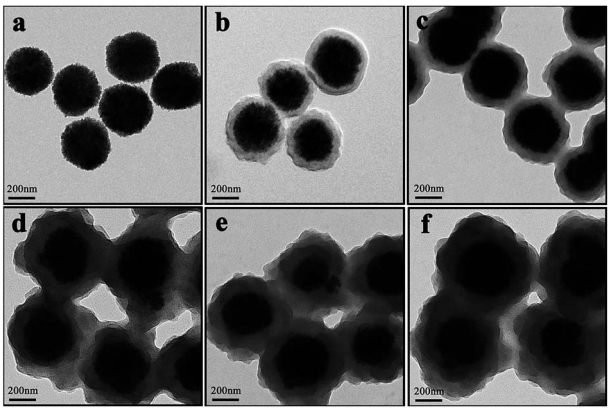

Fig. 1 HRTEM images of (a) Fe_3O_4, (b) Fe_3O_4@P4VP and Fe_3O_4@P4VP@MIL-100(Fe) core–shell after (c) 5, (d) 10, (e) 15, (f) 20 assembling cycles.

pyridine coordination, followed by reacting with 1,3,5-benzenetricarboxylic acid to complete each assembling cycle. The thickness of the MIL-100(Fe) shell was controlled by adjusting the assembling cycle. The MOF shells could be increased significantly to achieve a thickness ranging between 15 and 90 nm.

To further confirm the crystalline structures of the Fe_3O_4, Fe_3O_4@P4VP and Fe_3O_4@P4VP@MIL-100(Fe) microspheres, powder XRD were performed and the patterns are shown in Fig. 2. The diffraction peaks of Fe_3O_4 (Fig. 2a) agree with standard JCPDS 75-1609.39 indicating a face-centered cubic lattice. After coating with P4VP, the peaks of the core–shell Fe_3O_4@P4VP microspheres are almost the same as those for Fe_3O_4, because of the low-crystalline nature of the polymeric shell (Fig. 2b). However, after the introduction of the MIL-100(Fe) layer, several new peaks appeared on the XRD pattern (Fig. 2c). These new peak match the peaks present in the simulated MIL-100(Fe) pattern (Fig. S1†), which indicates that the formation of MIL-100(Fe) was successful.

The EDX elemental maps further support the successfulness of the synthesis of Fe_3O_4@P4VP@MIL-100(Fe), and that the iron MOF was well grafted on the surface of Fe_3O_4@P4VP (Fig. 3). The iron elemental maps of the Fe_3O_4@P4VP@MIL-100(Fe) also showed an excellent distribution of iron content on the surface. The existence of iron in the Fe_3O_4 core structure was also observed, as shown in Fig. 3.

The FTIR spectrum of the product is shown in Fig. 4. The relatively high intensity of the band at 592 cm^{-1} is characteristic of Fe–O vibrations. The characteristic absorption bands at 1707, 1250, and 1165 cm^{-1} correspond to the C=O stretching of the carboxylic group, to the in-plane bending of C–O–H, and to the –(C–O)H stretching, proving the existence of rich –COOH functional groups on the surface of the Fe_3O_4 particles. As for the Fe_3O_4@P(4-VP-DVB) microspheres, the characteristic absorptions at 1603, 1562, and 1417 cm^{-1} are attributed to the vibrational modes of the pyridine ring. The band at 1603 cm^{-1} corresponds to the stretching vibration absorption of the C–N bond, and the bands at around 1562 and 1417 cm^{-1} are attributed to the stretching vibration absorption of the C=C bond; this further proves the encapsulation of P4VP on the surface of the Fe_3O_4 particles. The peaks at 1435 and 1575 cm^{-1} are due to the stretching vibrations of the C–C bonds of the benzene ring, while the peaks at 1376 and 1618 cm^{-1} are

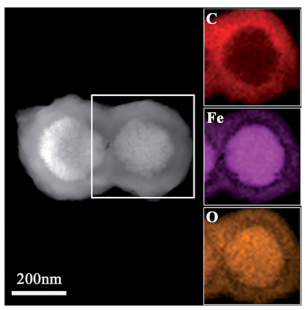

Fig. 3 The TEM images of the Fe_3O_4@P4VP@MIL-100(Fe) and EDX elemental maps of Fe, O and C, respectively.

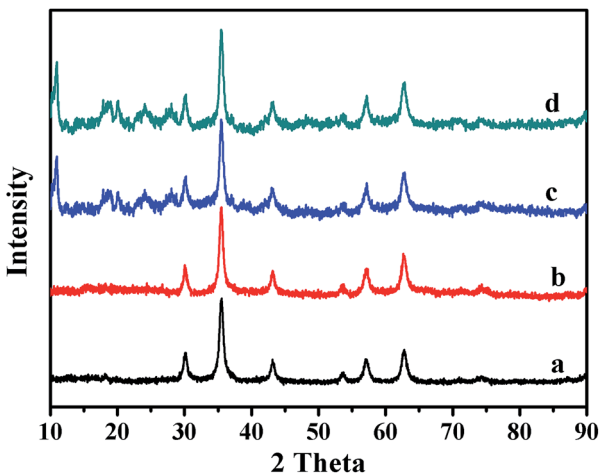

Fig. 2 XRD patterns of (a) Fe_3O_4, (b) Fe_3O_4@P4VP, (c) Fe_3O_4@P4VP@MIL-100(Fe) and (d) recycled Fe_3O_4@P4VP@MIL-100(Fe).

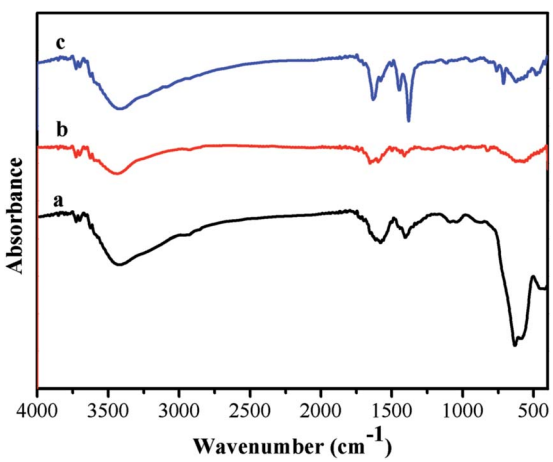

Fig. 4 FTIR spectra of (a) Fe_3O_4, (b) Fe_3O_4@P4VP and (c) Fe_3O_4@P4VP@MIL-100(Fe).

attributed to the C–O stretching vibrations of the carboxylic moiety, suggesting that MIL-100 (Fe) shell has been successfully grafted on the surface of Fe_3O_4@P4VP.

Surface area and pore size distribution were characterized by nitrogen adsorption/desorption experiment. The N_2 adsorption/desorption isotherms are shown in Fig. 5 and the curves are formed by the type I isotherms (Fig. 5). In addition, the isotherms are of type II at the range of high P/P_0. The surface area and pore volume of Fe_3O_4@P4VP@MIL-100(Fe) were calculated by the BET model and the values were determined to be 346.2 and 2.31 $m^3\ g^{-1}$, respectively. The surface area is significant improved, when compared to its Fe_3O_4@P4VP precursor, which has a surface area of 31.1 $m^2\ g^{-1}$.

TGA curves of Fe_3O_4, Fe_3O_4@P4VP and Fe_3O_4@P4VP@MIL-100(Fe) are shown in Fig. 6. For PAA modified Fe_3O_4 microspheres, the weight loss was about 17 wt% over two steps, attributed to the desorption of adsorbed water and PAA chains in Fe_3O_4 microspheres (Fig. 6a). The TGA curves of the Fe_3O_4@P4VP microspheres exhibited three steps of weight loss with 52 wt% of the initial weight remaining. Elimination of water, decomposition of the oligomeric structure and the desorption of P4VP shell correspond to the three weight losses (Fig. 6b). As expected, the mass loss of Fe_3O_4@P4VP@MIL-100(Fe) was lower than that of Fe_3O_4@P4VP, likely due to the formation of iron oxide through calcination (Fig. 6c).

The magnetic properties of Fe_3O_4 (PAA), Fe_3O_4@P4VP and Fe_3O_4@P4VP@MIL-100(Fe) were measured by vibrating sample magnetometry (VSM). All three samples exhibited superparamagnetism, presenting no remanence or coercitive forces (Fig. 7). The resultant magnetization saturation values of Fe_3O_4 (PAA), Fe_3O_4@P4VP and Fe_3O_4@P4VP@MIL-100(Fe) were 73.90, 47.35 and 28.21 emu g^{-1}, respectively, indicating strong magnetic response by the materials. The saturation magnetic moment of Fe_3O_4@P4VP and Fe_3O_4@P4VP@MIL-100(Fe) are lower than that of Fe_3O_4 because the P4VP and MOF shells are non-magnetic materials. Moreover, the saturation magnetic moment shows linear dependence on the content of magnetite. Therefore, the amount of P4VP and MIL-100(Fe) calculated according to the VSM results were 21.41 wt% and 40.42 wt%, respectively.

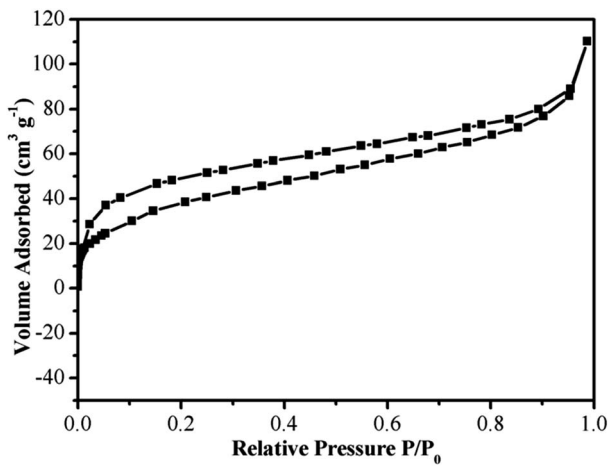

Fig. 5 N_2 adsorption–desorption isotherms of the Fe_3O_4@P4VP@MIL-100(Fe) catalyst.

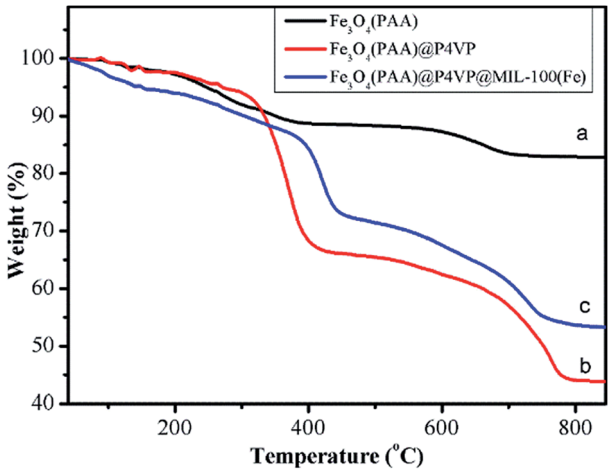

Fig. 6 TGA curves of (a) Fe_3O_4, (b) Fe_3O_4@P4VP and (c) Fe_3O_4@P4VP@MIL-100(Fe).

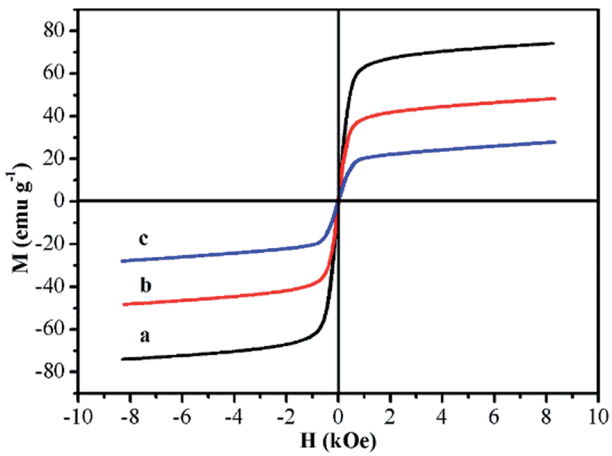

Fig. 7 Room-temperature magnetic hysteresis loops of (a) Fe_3O_4, (b) Fe_3O_4@P4VP and (c) Fe_3O_4@P4VP@MIL-100(Fe).

The catalytic activity of the synthesized Fe_3O_4@P4VP@MIL-100(Fe) toward the aerobic oxidation reaction was evaluated employing alcohol substrates, and using TEMPO as the radical initiator. No benzaldehyde was detected in the absence of the catalyst under our reaction conditions (Table 1, entry 1). Also, the employment of Fe_3O_4@P4VP as the catalyst failed to oxidize any benzyl alcohol to its corresponding aldehyde (Table 1, entry 2). Homogeneous iron catalysts were evaluated and almost quantitative conversion was observed. However, slightly lowered selectivity was observed due to the formation of benzoic acid (Table 1, entries 3 and 4). 82% conversion and 99% selectivity were achieved using MIL-100(Fe) MOF catalyst at 5 mol% catalyst loading (Table 1, entry 5). The amounts of MIL-100(Fe) and Fe_3O_4@P4VP@MIL-100(Fe) added in this reaction were 5 mol%, based on the same iron loading (Table 1, entries 5 and 6). The Fe_3O_4@P4VP@MIL-100(Fe) catalyst gave an excellent conversion and yield due to the efficient utilization of the

Table 1 Optimization of the aerobic oxidation reaction conditions[a]

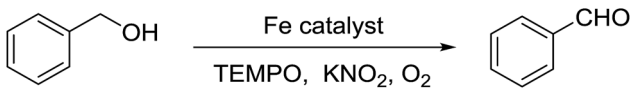

Entry	Catalyst	Solvent	Conv.[b]	Sel.[b]
1	—	CH_3CN	<5%	—
2	Fe_3O_4@P4VP	CH_3CN	<5%	—
3	$FeCl_3$	CH_3CN	99%	92%
4	$Fe(NO_3)_3$	CH_3CN	99%	93%
5	MIL-100(Fe)	CH_3CN	86%	99%
6	Fe_3O_4@P4VP@MIL-100(Fe)	CH_3CN	99%	99%
7[c]	Fe_3O_4@P4VP@MIL-100(Fe)	CH_3CN	36%	99%
8[d]	Fe_3O_4@P4VP@MIL-100(Fe)	CH_3CN	62%	99%
9	Fe_3O_4@P4VP@MIL-100(Fe)	$PhCH_3$	82%	99%
10	Fe_3O_4@P4VP@MIL-100(Fe)	THF	67%	99%
11	Fe_3O_4@P4VP@MIL-100(Fe)	EtOH	25%	99%

[a] Reaction conditions: 1.0 mmol of benzyl alcohol, 5 mol% of Fe_3O_4@P4VP@MIL-100(Fe) catalyst, 5.0 mL of solvent, 0.2 mmol of TEMPO, and 0.2 mmol of KNO_2; 60 °C, 12 h under 1 atm O_2. [b] Conversions and selectivities were calculated by GC-MS using nitrobenzene as the internal standard. [c] H_2O_2 was used as the oxidant. [d] Air was used as the oxidant.

porous MOF structure, which was coated as a nanolayer on the magnetic core. Hydrogen peroxide has been utilized as the oxidant, only low yield was obtained (Table 1, entry 7). Our reaction condition is not compatible with aqueous hydrogen peroxide oxidant. Furthermore, air was also tested as the low concentration form of oxygen and moderate yield was obtained (Table 1, entry 8). Further solvent screenings showed that CH_3CN is the most suitable solvent for the benzyl alcohol oxidation (Table 1, entries 6, 9–11). Aromatic solvents such as toluene gave slightly compromised yields, presumable due to their lower polarity (Table 1, entry 9). Moreover, oxygen containing solvents, such as THF and ethanol, were not suitable oxidation reaction solvent due to possible metal coordination (Table 1, entries 10 and 11).

Conversion was monitored over time employing various catalyst loadings of Fe_3O_4@P4VP@MIL-100(Fe); the results are summarized in Fig. 8. Relatively low conversion was observed at 1–3 mol% of catalyst loading, indicating the crucial role of the Fe-derived catalyst. However, conversion and yield were not satisfying until the catalyst loading was increased to 5 mol%. As a result, 5 mol% loading of Fe_3O_4@P4VP@MIL-100(Fe) was chosen to be the optimal reaction condition for future studies.

With the optimal reaction conditions in hand, several alcohol substrates were chosen to study the aerobic oxidation catalytic performance of Fe_3O_4@P4VP@MIL-100(Fe). Benzyl alcohol was transformed to the corresponding benzaldehyde in 99% yield after 12 h (Table 2, entry 1). For the aerobic oxidation of benzyl alcohol in presence of Fe_3O_4@P4VP@MIL-100(Fe) as the catalyst, the turnover number (TON) was calculated to be 20. Electron-rich benzyl alcohols, such as *p*-methyl benzyl alcohol and *p*-methoxy benzyl alcohol were reactive under the optimal reaction conditions, affording 99% and 92% yield, respectively

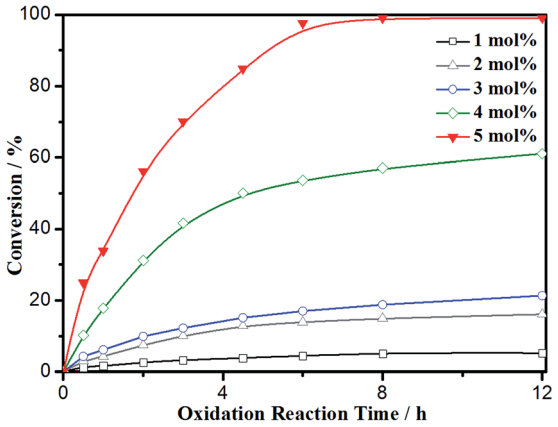

Fig. 8 Conversion *vs.* time at various core–shell catalyst loading.

Table 2 Aerobic oxidation of a variety of alcohols[a]

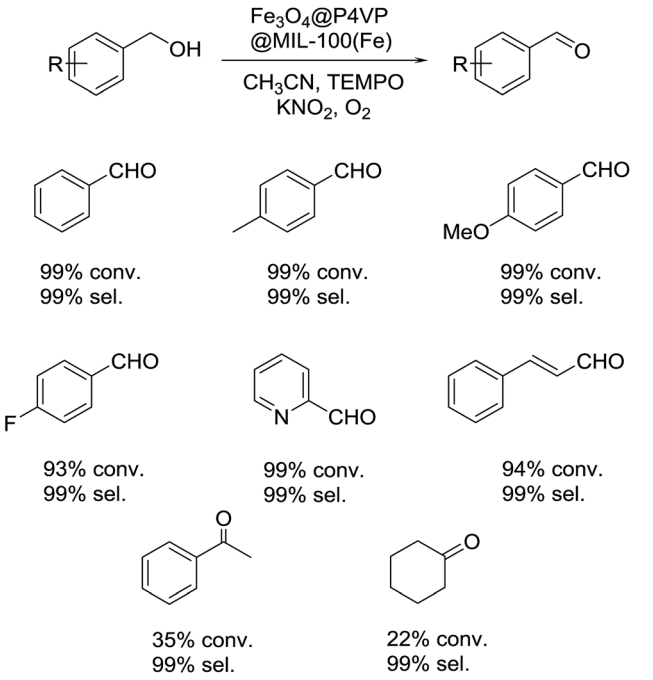

[a] Reaction conditions: 1.0 mmol of alcohol, 5 mol% of Fe_3O_4@P4VP@MIL-100(Fe) catalyst, 5.0 mL of solvent, 0.5 mmol of TEMPO, and 0.2 mmol of KNO_2; stirred at 60 °C for 12 h under 1 atm O_2.

(Table 2, entries 2 and 3). Alcohol substrates bearing electron-withdrawing functional groups were also tolerated; although a slightly lowered yield was observed for *p*-fluoro benzyl alcohols (Table 2, entry 4). The heterocyclic alcohol pyridin-2-ylmethanol was converted smoothly to its corresponding aldehyde in the presence of the Fe derived core–shell catalyst (Table 2, entry 5). Cinnamyl alcohol was also evaluated as an example of allylic alcohol; cinnamaldehyde was formed as the only product in 92% yield (Table 2, entry 6). In order to test the transformation of secondary alcohols to ketones, 1-phenylethanol and cyclohexanol were both tested; unfortunately, only low conversions were observed (Table 2, entries 7 and 8).

Fig. 9 Core–shell Fe-MOF catalyst recyclability test.

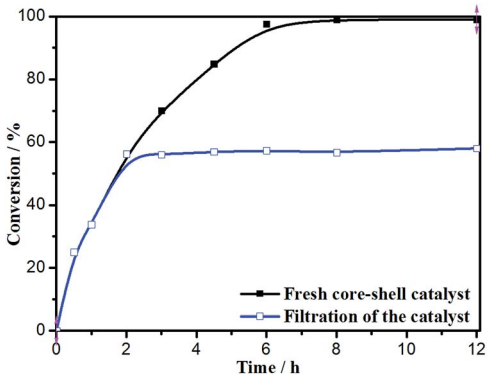

Fig. 10 Hot filtration test of Fe_3O_4@P4VP@MIL-100(Fe).

The recyclability of the catalyst was studied applying the optimal reaction conditions and utilizing 5 mol% of Fe_3O_4@P4VP@MIL-100(Fe) catalyst in acetonitrile (Fig. 9). The same batch of the Fe_3O_4@P4VP@MIL-100(Fe) catalyst was reused over ten reaction cycles; conversion and selectivity were retained at 99%, and the yield of benzaldehyde was compromised only slightly after ten cycles (Fig. 6). The retaining of high conversions and selectivities after ten cycles indicates that the core–shell MOF heterogeneous catalyst is highly stable. FT-IR and XRD spectra showed no significant difference between fresh Fe_3O_4@P4VP@MIL-100(Fe) and the batch analyzed after being used ten times (Fig. S2 and S3†).

The hot filtration test was conducted to confirm the heterogeneous nature of the catalytic aerobic oxidation (Fig. 10). The Fe_3O_4@P4VP@MIL-100(Fe) catalyst was isolated through magnet after 2 h of reaction and the mixture was stirred for another 10 h. Conversion to product stopped after the catalyst was removed. This result indicates that the strong covalent bond ensures the stability of Fe_3O_4@P4VP@MIL-100(Fe) material during the oxidation process. And that there is almost no Fe^{3+} leaching into the reaction solution, as also confirmed by ICP-AAS analysis.

4. Conclusions

During this study a novel magnetic core–shell Fe_3O_4@P4VP@MIL-100(Fe) catalyst was designed, prepared and fully characterized. The composite microspheres were composed by a magnetic Fe_3O_4(PAA) core, a P4VP middle layer, and a MIL-100(Fe) MOF shell. Taking advantage of their porous Fe-derived layer, the magnetic composite microspheres were utilized as an efficient catalyst for the selective aerobic oxidation of alcohols. A variety of alcohol substrates were tolerated under our optimized conditions. The initial catalytic activity of the Fe_3O_4@P4VP@MIL-100(Fe) catalyst was retained after at least ten consecutive reaction cycles. A hot filtration test suggested extremely low leaching of iron into the solution. Further applications of the prepared core–shell MOF catalyst are currently under investigation.

Acknowledgements

We thank the Science Research Foundation of Xijing University (Grant No. XJ16T02), the National Natural Science Foundation of China (No. 51673157) and the BUCT Fund for Disciplines Construction and Development (No. XK1529) for financial support.

Notes and references

1 (*a*) Q. Cao, L. M. Dornan, L. Rogan, N. L. Hughes and M. J. Muldoon, *Chem. Commun.*, 2014, **50**, 4524–4543; (*b*) J. Hou, Y. Luan, J. Tang, A. M. Wensley, M. Yang and Y. Lu, *J. Mol. Catal. A: Chem.*, 2015, **407**, 53–59.
2 B. Chen, L. Wang and S. Gao, *ACS Catal.*, 2015, **5**, 5851–5876.
3 (*a*) C. Parmeggiani and F. Cardona, *Green Chem.*, 2012, **14**, 547–564; (*b*) C. Qi, Y. Xiong, V. Eschenbrenner-Lux, C. Cong and J. A. Porco Jr, *J. Am. Chem. Soc.*, 2016, **138**, 798–801; (*c*) C. Qi, T. Qin, D. Suzuki and J. A. Porco Jr, *J. Am. Chem. Soc.*, 2014, **136**, 3374–3377; (*d*) Y. Luan, K. S. Barbato, P. N. Moquist, T. Kodama and S. E. Schaus, *J. Am. Chem. Soc.*, 2015, **137**, 3233–3236.
4 (*a*) M. Stratakis and H. Garcia, *Chem. Rev.*, 2012, **112**, 4469–4506; (*b*) Y. Luan, Y. Qi, Z. Jin, X. Peng, H. Gao and G. Wang, *RSC Adv.*, 2015, **5**, 19273–19278.
5 Z. Guo, B. Liu, Q. Zhang, W. Deng, Y. Wang and Y. Yang, *Chem. Soc. Rev.*, 2014, **43**, 3480–3524.
6 (*a*) M. A. Chari and K. Syamasundar, *Synthesis*, 2005, **5**, 0708–0710; (*b*) M. R. Farsani and B. Yadollahi, *J. Mol. Catal. A: Chem.*, 2014, **392**, 8–15; (*c*) Y. Kuang, Y. Nabae, T. Hayakawa and M. Kakimoto, *Appl. Catal., A*, 2012, **423–424**, 52–58; (*d*) P. Das, N. Aggarwal and N. R. Guha, *Tetrahedron Lett.*, 2013, **54**, 2924–2928.
7 P. R. Likhar, R. Arundhathi, S. Ghosh and M. L. Kantam, *J. Mol. Catal. A: Chem.*, 2009, **302**, 142–149.
8 J. Mao, X. Hu, H. Li, Y. Sun, C. Wang and Z. Chen, *Green Chem.*, 2008, **10**, 827–831.
9 R. G. Chaudhuri and S. Paria, *Chem. Rev.*, 2012, **112**, 2373–2433.
10 M. B. Gawande, A. Goswami, T. Asefa, H. Guo, A. V. Biradar, D. L. Peng, R. Zboril and R. S. Varma, *Chem. Soc. Rev.*, 2015, **44**, 7540–7590.
11 (*a*) C. Hui, C. Shen, J. Tian, L. Bao, H. Ding, C. Li, Y. Tian, X. Shi and H. J. Gao, *Nanoscale*, 2011, **3**, 701–705; (*b*)

Y. D. Chiang, S. Dutta, C. T. Chen, Y. T. Huang, K. S. Lin, J. C. S. Wu, N. Suzuki, Y. Yamauchi and K. C. W. Wu, *ChemSusChem*, 2015, **8**, 789–794; (*c*) Z. Dong, X. Le, C. Dong, W. Zhang, X. Li and J. Ma, *Appl. Catal., B*, 2015, **162**, 372–380; (*d*) X. Cui, W. Zuo, M. Tian, Z. Dong and J. Ma, *J. Mol. Catal. A: Chem.*, 2016, **423**, 386–392.

12 (*a*) Q. Zhang, I. Lee, J. B. Joo, F. Zaera and Y. Yin, *Acc. Chem. Res.*, 2013, **46**, 1816–1824; (*b*) P. Hu, J. V. Morabito and C. K. Tsung, *ACS Catal.*, 2014, **4**, 4409–4419; (*c*) Y. Long, M. Xie, J. Niu, P. Wang and J. Ma, *Appl. Surf. Sci.*, 2013, **277**, 288–292; (*d*) X. Zhang, J. Wu, G. Meng, X. Guo, C. Liu and Z. Liu, *Appl. Surf. Sci.*, 2016, **366**, 486–493; (*e*) Z. Sun, H. Li, G. Cui, Y. Tian and S. Yan, *Appl. Surf. Sci.*, 2016, **360**, 252–262.

13 W. Guo, G. Wang, Q. Wang, W. Dong, M. Yang, X. Huang, J. Yu and Z. Shi, *J. Mol. Catal. A: Chem.*, 2013, **378**, 344–349.

14 (*a*) S. Hübner, J. G. de Vries and V. Farina, *Adv. Synth. Catal.*, 2016, **358**, 3–25; (*b*) X. S. Zhao, X. Y. Bao, W. Guo and F. Y. Lee, *Mater. Today*, 2006, **9**, 32–39.

15 (*a*) H. C. Zhou, J. R. Long and O. M. Yaghi, *Chem. Rev.*, 2012, **112**, 673–674; (*b*) S. M. Cohen, *Chem. Sci.*, 2010, **1**, 32–36; (*c*) Y. Luan, M. Yang, Q. Ma, Y. Qi, H. Gao, Z. Wu and G. Wang, *J. Mater. Chem. A*, 2016, **4**, 7641–7649.

16 (*a*) J. Gascon, A. Corma, F. Kapteijn and F. X. L. I. Xamena, *ACS Catal.*, 2014, **4**, 361–378; (*b*) Y. Luan, Y. Qi, H. Gao, R. S. Andriamitantsoa, N. Zheng and G. Wang, *J. Mater. Chem. A*, 2015, **3**, 17320–17331; (*c*) C. Qi, D. Ramella, A. M. Wensley and Y. Luan, *Adv. Synth. Catal.*, 2016, **358**, 2604–2611.

17 (*a*) F. Ke, L. G. Qiu, Y. P. Yuan, X. Jiang and J. F. Zhu, *J. Mater. Chem.*, 2012, **22**, 9497–9500; (*b*) C. F. Zhang, L. G. Qiu, F. Ke, Y. J. Zhu, Y. P. Yuan, G. S. Xua and X. Jiang, *J. Mater. Chem. A*, 2013, **1**, 14329–14334; (*c*) F. Ke, L. Wang and J. Zhu, *Nanoscale*, 2015, **7**, 1201–1208; (*d*) W. W. Zhan, Q. Kuang, J. Z. Zhou, X. J. Kong, Z. X. Xie and L. S. Zheng, *J. Am. Chem. Soc.*, 2013, **135**, 1926–1933.

18 (*a*) D. W. Kim, H. G. Kim and D. H. Cho, *Catal. Commun.*, 2016, **73**, 69–73; (*b*) P. Horcajada, S. Surblé, C. Serre, D. Y. Hong, Y. K. Seo, J. S. Chang, J. M. Grenèche, I. Margiolakid and G. Férey, *Chem. Commun.*, 2007, 2820–2822; (*c*) A. Dhakshinamoorthy, M. Alvaro, P. Horcajada, E. Gibson, M. Vishnuvarthan, A. Vimont, J. M. Grenèche, C. Serre, M. Daturi and H. Garcia, *ACS Catal.*, 2012, **2**, 2060–2065.

19 H. Deng, X. Li, Q. Peng, X. Wang, J. Chen and Y. Li, *Angew. Chem., Int. Ed.*, 2005, **44**, 2782–2785.